JCI insight

RESEARCH ARTICLE

Inhibition of NADPH oxidase 2 (NOX2) prevents sepsis-induced cardiomyopathy by improving calcium handling and mitochondrial function

Leroy C. Joseph,[1] Dimitra Kokkinaki,[2,3] Mesele-Christina Valenti,[2] Grace J. Kim,[1] Emanuele Barca,[4,5] Dhanendra Tomar,[6] Nicholas E. Hoffman,[6] Prakash Subramanyam,[7] Henry M. Colecraft,[7] Michio Hirano,[4] Adam J. Ratner,[8] Muniswamy Madesh,[6] Konstantinos Drosatos,[2] and John P. Morrow[1]

[1]Department of Medicine, Columbia University College of Physicians and Surgeons, New York, New York, USA. [2]Metabolic Biology Laboratory, Center for Translational Medicine, Department of Pharmacology, Lewis Katz School of Medicine at Temple University, Philadelphia, Pennsylvania, USA. [3]The Molecular Basis of Human Diseases Graduate Program, Faculty of Medicine, University of Crete, Voutes, 71003 Heraklion-Crete, Greece. [4]Department of Neurology, Columbia University College of Physicians and Surgeons, New York, New York, USA. [5]Department of Clinical and Experimental Medicine, University of Messina, Messina, Italy. [6]Department of Medical Genetics and Molecular Biochemistry, Center for Translational Medicine, Lewis Katz School of Medicine at Temple University, Philadelphia, Pennsylvania, USA. [7]Department of Physiology and Cellular Biophysics, Columbia University College of Physicians and Surgeons, New York, New York, USA. [8]Departments of Pediatrics and Microbiology, New York University School of Medicine, New York, New York, USA.

Cardiomyopathy frequently complicates sepsis and is associated with increased mortality. Increased cardiac oxidative stress and mitochondrial dysfunction have been observed during sepsis, but the mechanisms responsible for these abnormalities have not been determined. We hypothesized that NADPH oxidase 2 (NOX2) activation could be responsible for sepsis-induced oxidative stress and cardiomyopathy. Treatment of isolated adult mouse cardiomyocytes with low concentrations of the endotoxin lipopolysaccharide (LPS) increased total cellular reactive oxygen species (ROS) and mitochondrial superoxide. Elevated mitochondrial superoxide was accompanied by depolarization of the mitochondrial inner membrane potential, an indication of mitochondrial dysfunction, and mitochondrial calcium overload. NOX2 inhibition decreased LPS-induced superoxide and prevented mitochondrial dysfunction. Further, cardiomyocytes from mice with genetic ablation of NOX2 did not have LPS-induced superoxide or mitochondrial dysfunction. LPS decreased contractility and calcium transient amplitude in isolated cardiomyocytes, and these abnormalities were prevented by inhibition of NOX2. LPS decreased systolic function in mice, measured by echocardiography. NOX2 inhibition was cardioprotective in 2 mouse models of sepsis, preserving systolic function after LPS injection or cecal ligation and puncture (CLP). These data show that inhibition of NOX2 decreases oxidative stress, preserves intracellular calcium handling and mitochondrial function, and alleviates sepsis-induced systolic dysfunction in vivo. Thus, NOX2 is a potential target for pharmacotherapy of sepsis-induced cardiomyopathy.

Authorship note: J.P. Morrow and K. Drosatos contributed equally to this work as co–senior authors.

Conflict of interest: The authors have declared that no conflict of interest exists.

Submitted: March 29, 2017
Accepted: July 25, 2017
Published: September 7, 2017

Reference information:
JCI Insight. 2017;2(17):e94248. https://doi.org/10.1172/jci.insight.94248.

Introduction

Sepsis is a common cause of death in developed countries (1). Cardiac involvement frequently complicates sepsis. One hospital-based study found that 43% of patients with bacteremia had positive serum troponin, indicating myocardial damage (2). Clinical studies have shown that if sepsis causes cardiac systolic dysfunction (also called sepsis-induced cardiomyopathy) the mortality rate increases up to 80%, compared with a 20% mortality rate for sepsis with normal systolic function (3, 4). Sepsis can also cause abnormal cardiac electrophysiology, as indicated by the fact that patients with sepsis often have abnormal electrocardiograms and/or arrhythmias (5, 6). Atrial fibrillation is 6 times more com-

mon in patients admitted to the ICU with sepsis compared with other diagnoses (7). Currently, there is no therapy for sepsis-induced cardiomyopathy.

Introduction of live bacteria or injection of the bacterial endotoxin lipopolysaccharide (LPS) have been used for animal models of sepsis. Studies of human blood metabolites show that LPS injection correlates with the abnormalities seen in sepsis (8). A variety of mechanisms have been proposed to explain cardiomyopathy during sepsis, including increased reactive oxygen species (ROS) as an important part of the pathophysiology (9, 10). Mitochondrial dysfunction has been a consistent finding in sepsis models, with decreased mitochondrial oxidative phosphorylation and decreased transcription of mitochondrial genes (11–13). Abnormalities of intracellular calcium handling have also been observed in cardiomyocytes from animal models of sepsis (14–17). Multiple stress-related kinases are activated in the heart during sepsis, including protein kinase C (PKC) and c-Jun N-terminal kinase (JNK) (18, 19). However, there is no unified explanation of these multiple cardiac abnormalities. Specifically, the mechanisms responsible for increased oxidative stress and mitochondrial dysfunction in the heart during sepsis remain obscure, and it is not understood how these abnormalities may be related to abnormal intracellular calcium handling. We hypothesized that NADPH oxidase 2 (NOX2) activation is the primary mechanism causing systolic dysfunction during sepsis.

Results

LPS increases oxidative stress in cardiomyocytes and causes mitochondrial dysfunction. We quantified oxidative stress in ventricular cardiomyocytes, and found that low concentrations of LPS increased total cellular ROS after 1-hour exposure (as indicated by 2′,7′-dichlorofluorescin diacetate [DCF] fluorescence). There was a stepwise increase in ROS with escalating doses of LPS (Figure 1A). LPS also increased mitochondrial superoxide significantly in cardiomyocytes, as indicated by MitoSOX Red fluorescence, which is a mitochondrial superoxide indicator (Figure 1B). Mitochondria can produce several species of ROS, but superoxide is the most proximal (20). To better characterize the mitochondrial abnormalities induced by LPS, we quantified the mitochondrial inner membrane potential using tetramethylrhodamine methyl ester (TMRM) (21). Normally, the mitochondrial inner membrane has a voltage gradient, with the interior negative in relation to the cytosol. LPS causes partial depolarization of the mitochondrial inner membrane potential, an indication of mitochondrial dysfunction (Figure 1C). Partial depolarization of the inner membrane potential can be caused by excessive mitochondrial calcium uptake (22). To evaluate calcium overload as a cause of mitochondrial dysfunction, we quantified mitochondrial calcium levels during LPS treatment and found that LPS caused mitochondrial calcium overload, in a dose-responsive manner (Figure 1D).

To determine the effects of LPS on mitochondrial oxidative phosphorylation, we used the H9c2 cardiomyoblast cell line. Cells were exposed to LPS and then mitochondrial oxygen consumption was quantified with a Seahorse system. The results show that LPS causes a significant decrease in maximal mitochondrial oxidative phosphorylation (induced by pharmacologic uncoupling) after a 2-hour exposure (Figure 1E). There was no significant difference after 1-hour exposure, indicating that mitochondria are able to function in the early stages of LPS exposure despite increased oxidative stress.

LPS increases calcium sparks, and RyR inhibition reduces mitochondrial dysfunction and oxidative stress. Previous work has shown that sepsis-induced cardiomyopathy is characterized by increased sarcoplasmic reticulum calcium leak (23). To determine if LPS is sufficient to increase sarcoplasmic reticulum calcium leak independently of immune response, we measured sparks (spontaneous calcium release events) in isolated cardiomyocytes. This showed that 1 hour of LPS exposure is sufficient to cause a significant increase in sparks (Figure 2, A–C). To verify that ryanodine receptor–mediated (RyR-mediated) calcium leak causes mitochondrial calcium overload, we used dantrolene, which inhibits opening of RyR channels. Dantrolene prevented the increase in mitochondrial calcium caused by LPS. Dantrolene also reduced oxidative stress and blunted the partial depolarization of the inner membrane (Figure 2, D–G).

In cardiac ischemia/reperfusion, it is known that mitochondrial calcium overload causes opening of the mitochondrial permeability transition pore (mPTP), contributing to oxidative stress and cardiac dysfunction (24). To determine if mPTP opening could be involved in sepsis, we inhibited the opening of the mPTP with cyclosporin A. Cyclosporin A reduces mitochondrial superoxide after LPS exposure and offers some protection from mitochondrial depolarization (Figure 2, D–G). We infer that LPS-induced sarcoplasmic reticulum calcium leak leads to mitochondrial calcium overload and opening of the mPTP, which contributes to mitochondrial depolarization and superoxide production.

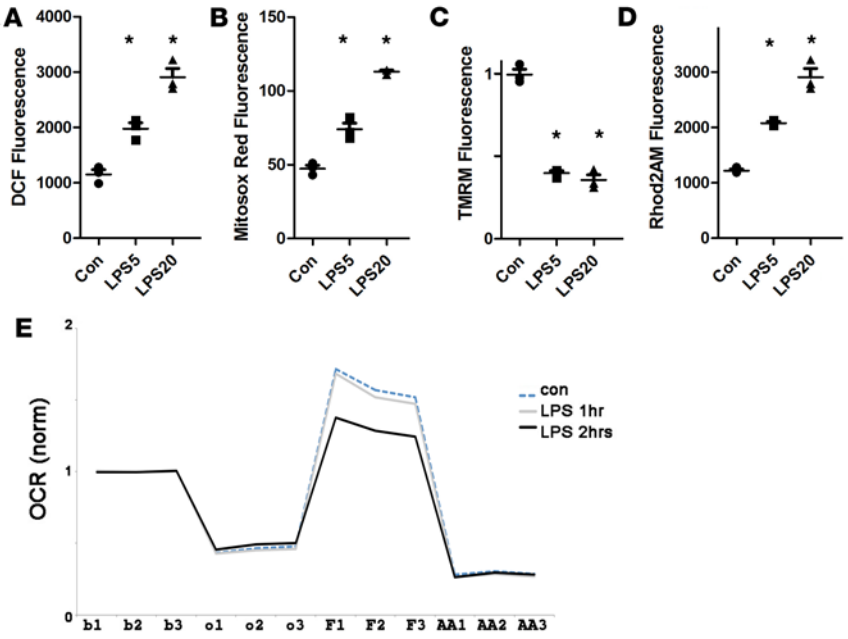

Figure 1. LPS increases oxidative stress in cardiomyocytes and causes mitochondrial dysfunction. (**A**) Representative experiment done with WT adult mouse ventricular myocytes (AMVMs) in triplicate wells, 2,000 cells/well; height is DCF fluorescence minus background, arbitrary units, in live cells, mean + SEM. LPS increases ROS significantly. LPS = lipopolysaccharide 5 or 20 ng/ml as noted, 1-hour exposure. (**B**) Cardiomyocytes from the same experiment using MitoSOX Red readout, arbitrary units, to indicate mitochondrial superoxide. (**C**) Cardiomyocytes from the same experiment using TMRM readout to indicate mitochondrial inner membrane depolarization. (**D**) Cardiomyocytes from the same experiment using Rhod 2-AM readout, arbitrary units, to indicate mitochondrial calcium load. For panels **A**–**D**, means are significantly different by ANOVA; *significantly different from control by post-hoc test. (**E**) Maximum oxygen consumption rate (OCR) is decreased in H9c2 cells by LPS. Measurements from 3 time points were obtained under each condition, using triplicate wells. $P = 0.014$ for comparison of control with 2-hour LPS at the FCCP step (to stimulate maximum oxygen consumption). b, baseline; o, oligomycin; F, FCCP; AA, antimycin-A and rotenone.

NOX2 activation is required for LPS-induced ROS. Next, we investigated the mechanism by which LPS causes increased oxidative stress and sarcoplasmic reticulum calcium leak. Mitochondria are a major source of ROS in cardiomyocytes, but NOX isoforms have also been implicated in the pathophysiology of sepsis (25). Furthermore, NOX2 activation is known to increase sarcoplasmic reticulum calcium release (26). We used the lucigenin assay to quantify NOX2 production of superoxide, which confirmed that LPS rapidly activates NOX2 in cardiomyocytes (Figure 3A). The NOX inhibitor apocynin prevented NOX activation by LPS (Figure 3A). We also used a NOX2 inhibitor peptide, gp91ds-tat, to ensure specificity, confirming that NOX2 is the source of LPS-stimulated superoxide (Figure 3A). It is known that NOX2 can be activated by PKC isoforms in cardiomyocytes (27). To determine if PKC activation is required for the pathophysiology caused by LPS, we used the broad-spectrum PKC inhibitor Go6983, which prevented NOX activation by LPS (Figure 3A).

We used the NOX2 inhibitor peptide to evaluate the contribution of NOX2 to LPS-induced oxidative stress. The inhibitor peptide reduced, but did not normalize, the increase in oxidative stress caused by LPS (Figure 3, B and C). The inhibitor peptide prevented the decrease in inner membrane potential and prevented the increase in mitochondrial calcium (Figure 3, D and E). This shows that NOX2 activation contributes to LPS-induced oxidative stress and mitochondrial dysfunction. The PKC inhibitor Go6983 reduced total and mitochondrial ROS caused by LPS (Figure 3, B and C), consistent with PKC being upstream of NOX activation. The PKC inhibitor also prevented the decrease in mitochondrial membrane potential and mitochondrial calcium overload (Figure 3, D and E).

To confirm the pharmacologic data, we used NOX2-KO mice, which did not have increased oxidative stress after exposure to LPS (Figure 3, F and G). In addition, NOX2-KO cardiomyocytes did not have mitochondrial depolarization or mitochondrial calcium overload after LPS treatment (Figure 3, H and I). This indicates that NOX2 activation is necessary for LPS-induced oxidative stress and mitochondrial dysfunction in cardiomyocytes.

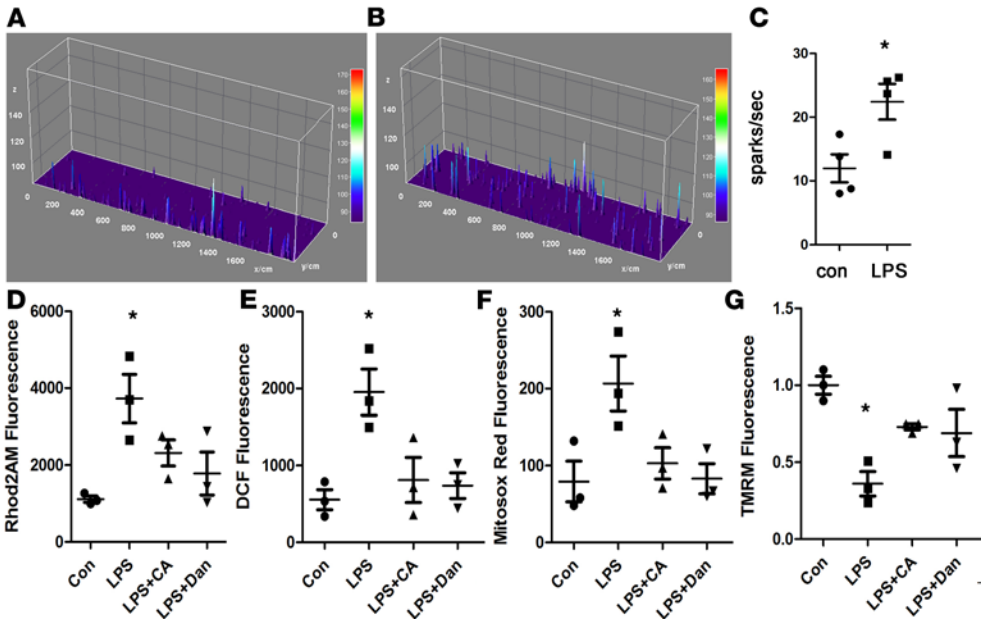

Figure 2. LPS increases calcium sparks, and RyR inhibition reduces LPS-induced ROS and mitochondrial dysfunction. (**A**) Representative image of calcium sparks in WT isolated adult mouse ventricular myocytes. (**B**) Image of calcium sparks in WT cardiomyocytes exposed to LPS for 1 hour. (**C**) Quantification of sparks in WT cardiomyocytes exposed to LPS for indicated time. *n* = 4 independent cardiomyocyte isolations. *Significantly different from control by unpaired *t* test. (**D**) Mitochondrial calcium in WT cardiomyocytes, Rhod 2-AM signal minus background, mean ± SEM, *n*= 3 independent cardiomyocyte isolations. (**E**) Cellular ROS in WT cardiomyocytes, DCF fluorescence, mean ± SEM, *n*= 3 independent cardiomyocyte isolations. (**F**) Mitochondrial ROS in WT cardiomyocytes, MitoSOX Red fluorescence, mean ± SEM, *n* = 3 independent cardiomyocyte isolations. (**G**) Mitochondrial inner membrane potential in WT cardiomyocytes, TMRM fluorescence, mean ± SEM, *n* = 3 independent cardiomyocyte isolations. For panels **D**–**G**, means are significantly different by ANOVA; *significantly different from control by post-hoc test. LPS = 20 ng/ml, 1-hour exposure. Dan, 1 μM dantrolene; CA, 20 μM cyclosporin A.

LPS rapidly reduces contractility and causes abnormal calcium transients in cardiomyocytes, which is prevented by NOX2 inhibition. Prior work has shown that cardiomyocytes from mice injected with LPS have abnormal calcium transients, with lower amplitude and longer decay phase (return to baseline) (23). To determine if LPS exposure itself is sufficient to cause decreased contractility and abnormal calcium transients, rather than activation of the immune system, we exposed isolated WT cardiomyocytes to LPS for 1 hour and then measured contractility and calcium transients. LPS caused a significant decrease in contractility in ventricular cardiomyocytes after a 1-hour exposure (Figure 4, A and C). Calcium transients from cardiomyocytes exposed to LPS had significantly decreased amplitude, and a longer decay phase as quantified by the time constant tau (Figure 4, B and D). We evaluated the effect of inhibition of NOX2 on isolated cardiomyocyte contractility and calcium transients. Apocynin prevented the decrease in contractility and calcium transient amplitude induced by LPS exposure, indicating that NOX2 activation is necessary for abnormal calcium handling after LPS exposure (Figure 4, C and D). The same effects were evident at faster pacing rates (Supplemental Figure 1; supplemental material available online with this article; https://doi.org/10.1172/jci.insight.94248DS1).

Decreased calcium transient amplitude is consistent with either decreased sarcoplasmic reticulum calcium stores or decreased fractional release. We evaluated sarcoplasmic reticulum calcium with the caffeine method. These results showed no significant change in sarcoplasmic reticulum calcium load 1 hour after LPS exposure, suggesting that decreased fractional release is responsible (Supplemental Figure 2). In summary, these results show that LPS is sufficient to decrease contractility and impair calcium handling in isolated cardiomyocytes in a NOX-dependent manner.

NOX2 inhibition is cardioprotective in a mouse model of sepsis. To assess the significance of NOX2 activation in septic cardiac dysfunction in vivo, we used a mouse model of LPS-induced endotoxemia (11, 28). Wild-type (WT) mice were injected with LPS, which is known to decrease cardiac contractility, and then we assessed cardiac function by echocardiography. Inhibition of NOX activity with apocynin has a protective

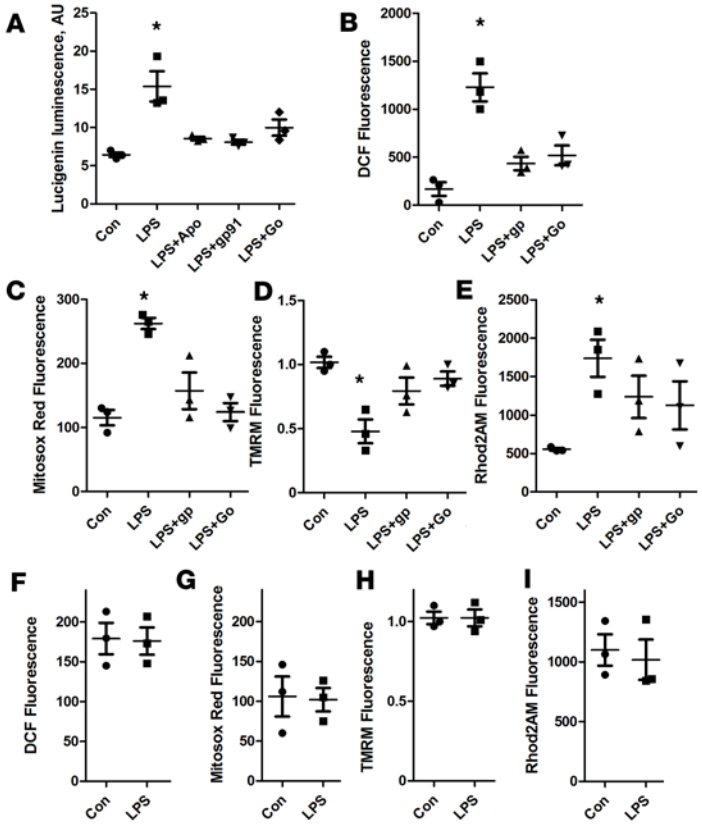

Figure 3. NOX2 activation is required for LPS-induced oxidative stress. (**A**) One-hour exposure to LPS increases NOX activity and NOX or PKC inhibition prevents the increase in NOX activity. Height is lucigenin luminescence, in arbitrary units, from WT mouse cardiomyocytes lysates, *n* = 3 independent cardiomyocyte isolations. (**B**) PKC and NOX2 inhibitors prevent LPS-induced ROS in isolated WT cardiomyocytes. DCF fluorescence minus background, in live cells, mean ± SEM. *n* = 3 independent cardiomyocyte isolations. (**C**) PKC and NOX2 inhibitors prevent LPS-induced mitochondrial ROS in isolated WT cardiomyocytes. MitoSOX Red fluorescence minus background, in live cells, mean ± SEM, *n* = 3 independent cardiomyocyte isolations. (**D**) PKC and NOX2 inhibitors prevent the loss of mitochondrial inner membrane potential in isolated WT cardiomyocytes. TMRM readout in live cells, mean ± SEM, *n* = 3 independent cardiomyocyte isolations. (**E**) PKC and NOX2 inhibitors prevent the increase in mitochondrial calcium in isolated WT cardiomyocytes. Rhod 2-AM readout in live cells, mean ± SEM, *n* = 3 independent cardiomyocyte isolations. (**F**) LPS does not induce ROS in isolated NOX2-KO cardiomyocytes. DCF fluorescence minus background, in live cells, mean ± SEM, *n* = 3 independent cardiomyocyte isolations. (**G**) LPS does not induce mitochondrial ROS in isolated NOX2-KO cardiomyocytes. MitoSOX Red fluorescence minus background, in live cells, mean ± SEM. *n* = 3 independent cardiomyocyte isolations. (**H**) LPS does not decrease the mitochondrial inner membrane potential in isolated NOX2-KO cardiomyocytes. TMRM fluorescence minus background, in live cells, mean ± SEM. *n* = 3 independent cardiomyocyte isolations. (**I**) LPS does not increase mitochondrial calcium in isolated NOX2-KO cardiomyocytes. Rhod 2-AM fluorescence minus background, in live cells, mean ± SEM. *n* = 3 independent cardiomyocyte isolations. For all panels, means are significantly different by ANOVA; *significantly different from control by post-hoc test. LPS = 20 ng/ml, 1-hour exposure; apo = 200 μM apocynin; Go = 5 μm Go6983 PKC inhibitor; gp91 = gp91ds-tat NOX2 inhibitor peptide.

effect on systolic function after LPS injection (Figure 5, A–C and Supplemental Table 1). Apocynin also prevented the increase in ventricular brain natriuretic peptide (BNP) expression, a marker of heart failure (Figure 5D). Plasma levels of IL-6 and TNF-α were not improved by apocynin, indicating that the benefit of NOX2 inhibition is not mediated by reduction of systemic inflammation (Figure 5, E and F).

In addition, NOX inhibition prevented activation of cardiac JNK (Figure 5G). We have previously shown that the JNK pathway is activated in the heart during sepsis and is responsible for downregulation of genes required for normal mitochondrial respiration (13, 29). Consistent with this prior work, NOX inhibition prevented abnormal transcriptional regulation induced by LPS. LPS reduced cardiac mRNA levels of several genes that are critical for metabolism and mitochondrial function: Pparα, Pgc1α, and Cpt1β. Apocynin prevented downregulation of these genes (Figure 5H). Not all mitochondrial genes were downregulated by LPS. We found that LPS increased mRNA expression of uncoupling protein 2 (Ucp2) and Ucp3 in the heart, and these levels were normalized by apocynin (Supplemental Figure 3).

Staining of ventricular tissue with dihydroethidium demonstrated that LPS causes a significant increase in oxidative stress, and this was prevented by apocynin (Figure 6). Histology also showed that LPS increased cardiac NADPH levels, and this was not prevented by apocynin. Since NOX2 activation would tend to consume NADPH and increase levels of $NADP^+$, there must be compensatory mechanisms to increase NADPH after exposure to LPS. For example, NADPH is used in many anabolic reactions, so a decrease in anabolic metabolism could increase tissue levels. Collectively, these data suggest that NOX2 activation is the major mechanism causing oxidative stress and systolic dysfunction in the early stages of sepsis.

PKC and NOX2 inhibition are cardioprotective in a mouse model of sepsis. Since our data show that PKC activation could be upstream of NOX2 activation in isolated cardiomyocytes (Figure 3), we evaluated PKC isoforms in membrane preparation lysates from ventricular tissue of mice injected with LPS or vehicle control. PKCα showed a nonsignificant trend towards activation, and PKCβ and PKCδ were significantly activated in the heart after LPS exposure (Figure 7, A and B). Interestingly, PKCβ has been identified as an activator of NOX during cardiac lipotoxicity (30). There was also a corresponding decrease in membrane-

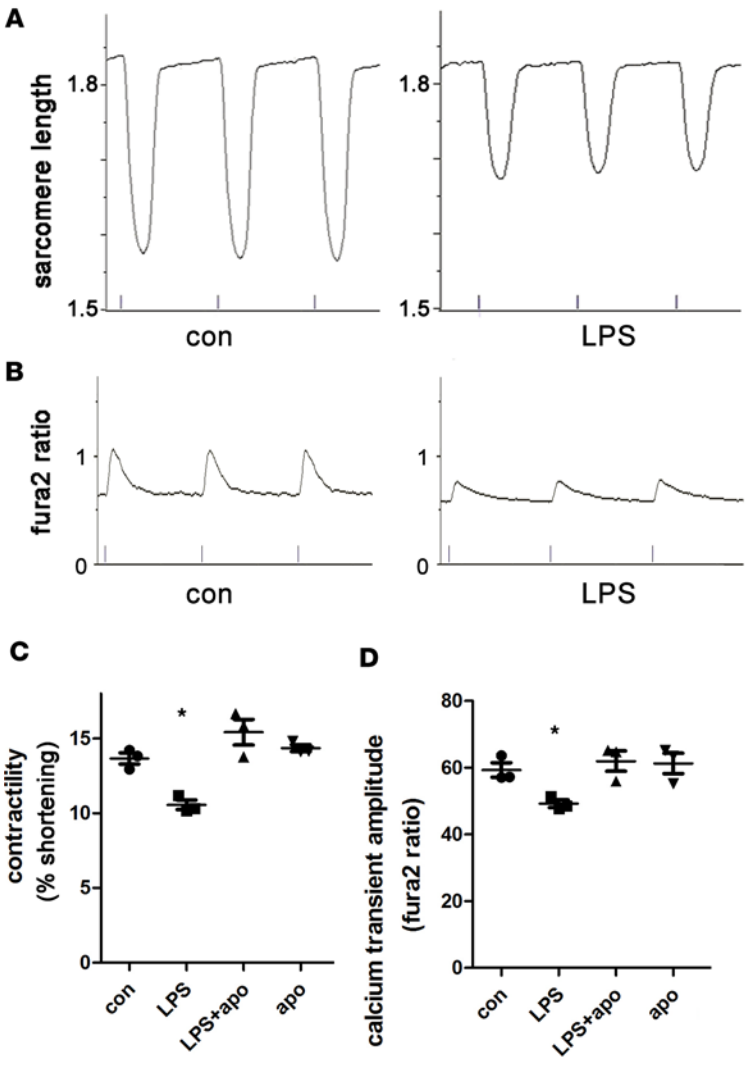

Figure 4. LPS rapidly reduces contractility and causes abnormal calcium transients in cardiomyocytes, which is prevented by NOX2 inhibition. (**A**) Representative raw data of isolated WT cardiomyocyte contractility, sarcomere length in μm, in cardiomyocytes under control conditions or treated with LPS. (**B**) Representative calcium transients from WT cardiomyocytes under control conditions or treated with LPS. (**C**) Graph of isolated cardiomyocyte contractility paced at 1 Hz, as percentage sarcomere shortening from baseline sarcomere length, for WT cardiomyocytes treated with LPS and/or apocynin (apo), mean ± SEM. (**D**) Graph of maximum amplitude of calcium transients, expressed as percentage change from baseline for WT cardiomyocytes treated with LPS and/or apocynin (apo), mean ± SEM. For panels **C** and **D**, *n* = 3 different cardiac isolations (5–10 cells averaged per group for each isolation); the means are different by ANOVA; *significantly different from control by post-hoc test.

bound PKCε (Figure 7B). We evaluated the in vivo benefit of PKC inhibition using the same animal model of sepsis. The broad-spectrum PKC inhibitor Ro-31-8220 prevented cardiac systolic function after LPS injection, consistent with PKC activation upstream of NOX2 activation (Figure 7, C and D).

Live bacteria model of sepsis confirms that PKC and NOX2 inhibition are protective. To confirm the results of the LPS injection model, we used an established model of polymicrobial sepsis, cecal ligation and puncture (CLP) (31). Serial echocardiograms demonstrated a gradual reduction in ejection fraction after CLP (Supplemental Figure 4). We confirmed that NOX activity is increased in the heart after CLP, and apocynin blunts this increase in NOX activity (Figure 8A). We also confirmed that PKC isoforms were activated in the hearts of mice after CLP (Supplemental Figure 4). Notably, PKCβ was activated in both the LPS injection and CLP mouse models. Both the PKC inhibitor and apocynin had a protective effect on cardiac systolic function in the CLP model (Figure 8, B and C). Consistent with the LPS injection data, neither treatment had a significant antiinflammatory effect in the CLP model based on cardiac tissue inflammatory gene expression (Figure 8D). Metabolic gene expression in the heart was improved by the PKC inhibitor in the CLP model (Figure 8E).

To evaluate apocynin as a therapy after the onset of sepsis, another group of mice were treated with apocynin 9 hours after CLP surgery, since this is the time point that showed a consistent reduction in ejection fraction. At 12 hours after CLP we evaluated the cardiac function, and then sacrificed the mice. Apocynin given after the onset of sepsis showed a trend toward improved ejection fraction (Supplemental Figure 5).

We also evaluated cardiac function 24 hours after CLP surgery. For this experiment we gave the first dose of apocynin during CLP and the second dose at 12 hours after CLP; 24 hours after CLP we evaluated

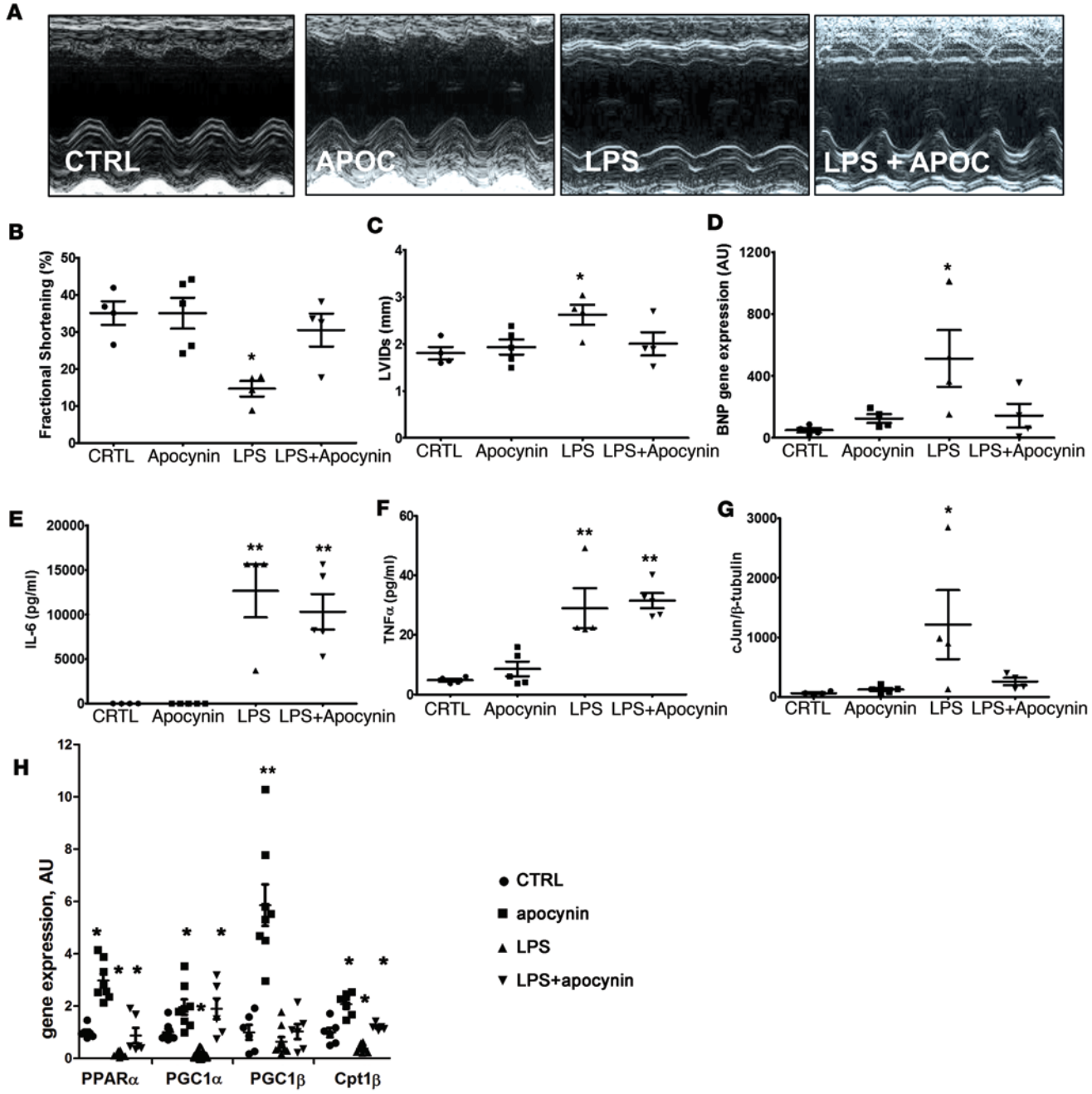

Figure 5. NOX2 inhibition prevents cardiomyopathy in vivo but does not prevent inflammation. (**A**) Representative M-mode echocardiograms. (**B**) Graph of fractional shortening (FS), $n = 4–5$ mice. (**C**) Graph of left ventricular internal dimensions during systole (LVIDs), $n = 4–5$ mice. (**D**) Graph of ventricular BNP mRNA levels, $n = 4–5$ mice. (**E** and **F**) Plasma levels of IL-6 and TNF-α, $n = 4–5$ mice. (**G**) Graph of multiplex protein analysis for p-JNK adjusted relative to β-tubulin. $n = 4–5$ mice. (**H**) Graph of metabolic gene expression from ventricular tissue. $n = 6–8$ heart samples. All panels show data from C57BL/6 mice treated with saline (control), apocynin, LPS, or combination of LPS and apocynin. $^*P < 0.05$, $^{**}P < 0.01$ compared with control by ANOVA with post-hoc testing.

the cardiac function with echocardiography. Mice in the sham and CLP groups received vehicle (DMSO) at both time points as a control. We also took blood at 24 hours after CLP to measure white blood cell (WBC) count, another measure of immune system activation. Apocynin preserved the ejection fraction at 24 hours (Supplemental Figure 6, A and B). Both the CLP vehicle group and the CLP+apocynin group had a decrease in WBC compared with sham (Supplemental Figure 6C). However, apocynin did not improve mortality (Supplemental Figure 6D). Additional work did not show a difference in P-ERK (a marker of activation of the ERK stress kinase) after CLP (Supplemental Figure 7).

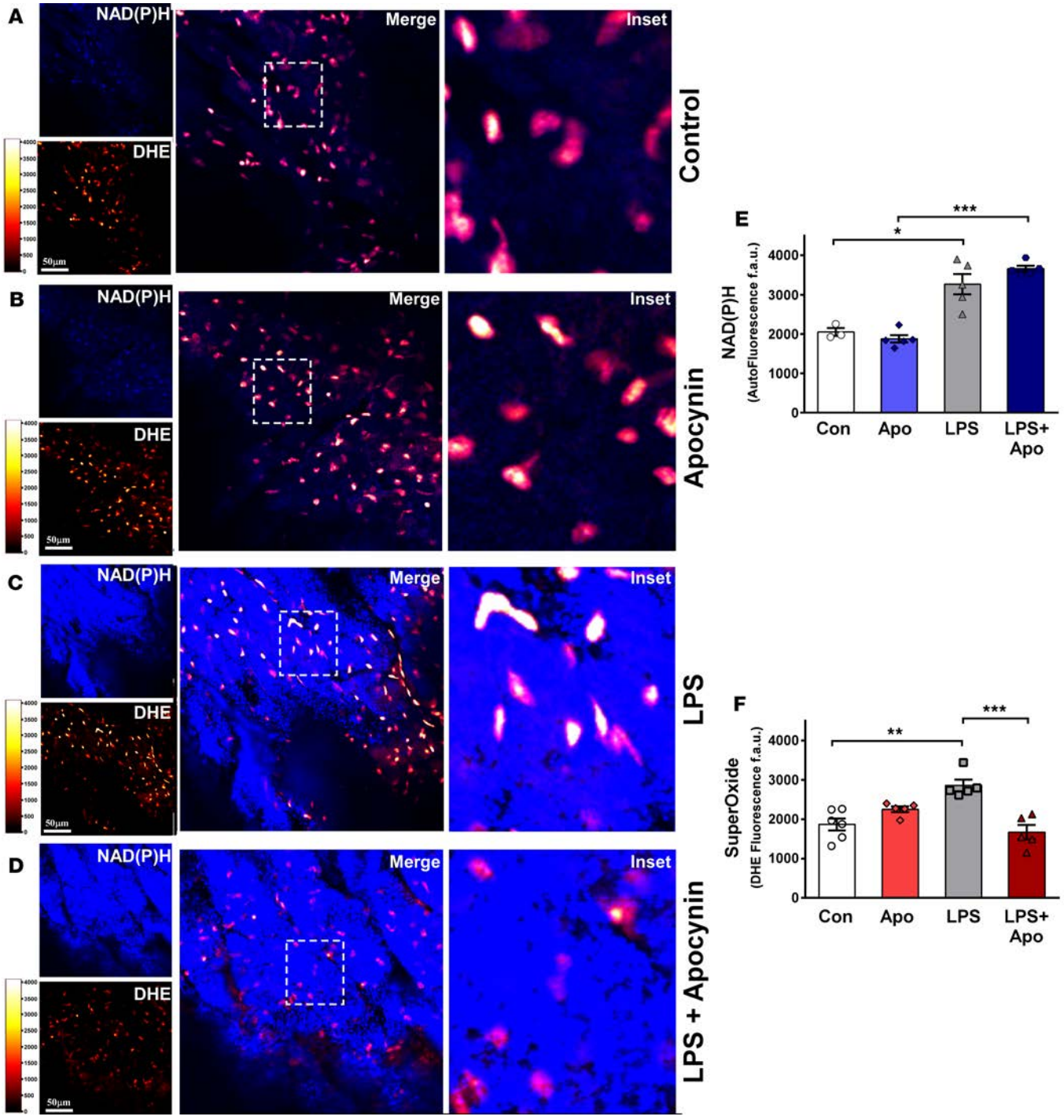

Figure 6. Apocynin reduces superoxide in cardiac tissue (left ventricle). (**A**) Representative confocal images of superoxide detection by dihydroethidium (DHE) and NADPH autofluorescence (blue color) in left ventricular tissue slices from control mice. DHE signal is indicated by the red to white range indicator. Scale bars: 50 μm, with high magnification (×2 zoom of merged images) inset indicated by dashed square. (**B**) Representative confocal image from apocynin-treated tissue for superoxide and NADPH. Same scale as **A**. (**C**) Representative confocal image from LPS-treated tissue for superoxide and NADPH. (**D**) LPS+apocynin–treated representative confocal image. (**E**) Quantification of NADPH signal from control, apocynin, LPS, and LPS+apocynin heart samples. (**F**) Quantification of superoxide signal from control, apocynin, LPS, and LPS+apocynin heart samples. n = 3–6 mice/group. $^{*}P < 0.05$, $^{**}P < 0.01$, $^{***}P < 0.001$ by ANOVA with post-hoc testing.

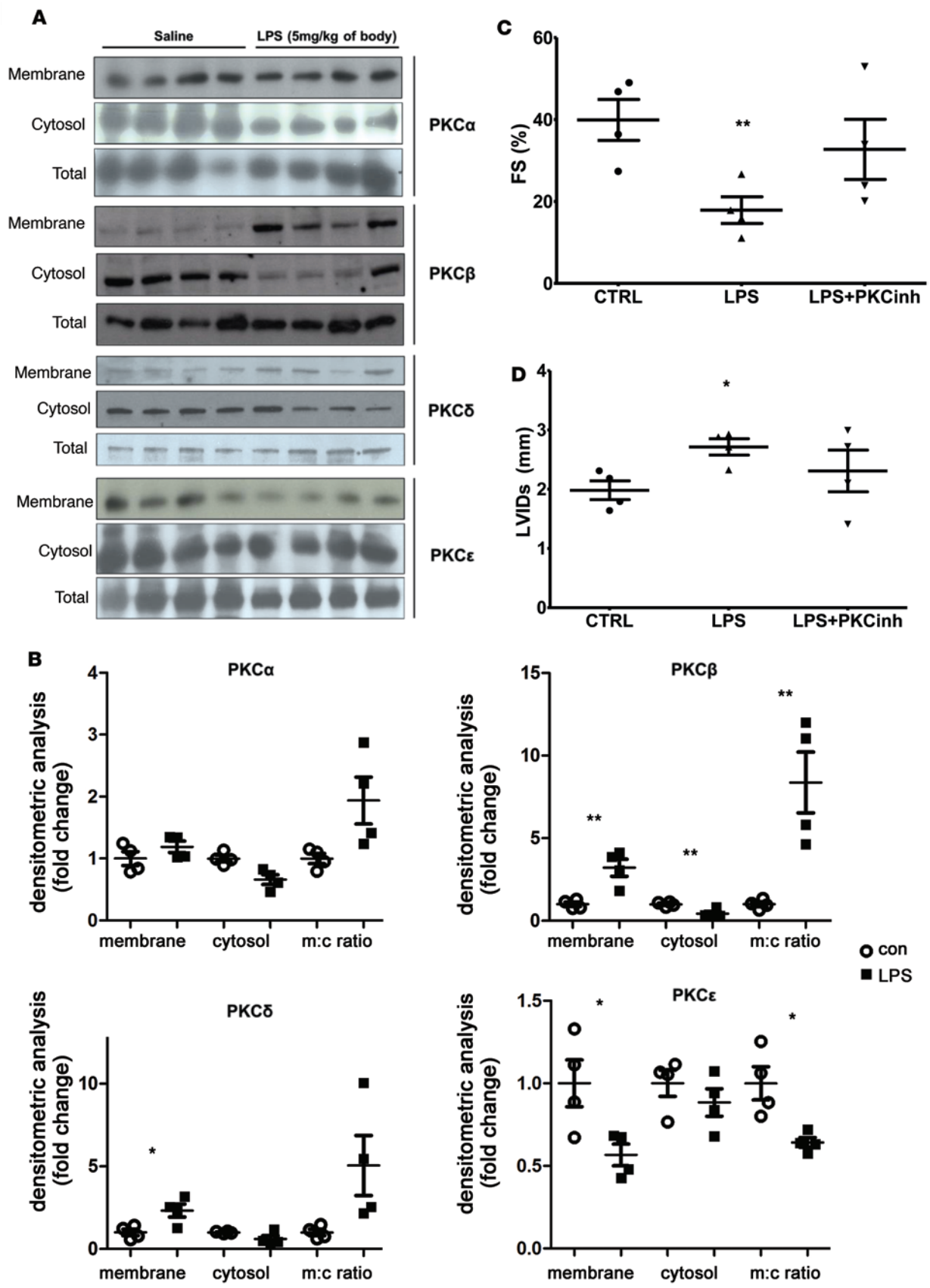

Figure 7. LPS activates PKCβ and PKCδ, and PKC inhibition improves cardiac function in vivo. (**A**) Western blots of PKC isoforms, membrane and cytosolic fraction, from ventricular tissue of mice treated with LPS or vehicle control. (**B**) Densitometric analysis of PKC Western blots, in relative units. $*P < 0.05$, $**P < 0.01$ by unpaired *t* test (control vs. LPS for each fraction). Open circles are control, squares are LPS treatment. (**C**) Fractional shortening (FS) by echocardiogram, and (**D**) left ventricular internal diameter during systole (LVIDs). $*P < 0.05$, $**P < 0.01$ by ANOVA with post-hoc testing. All data are from C57BL/6 mice treated with saline, LPS, and/or PKC inhibitor Ro-31-8220, $n = 4$.

Discussion

Sepsis is a common disease with a high mortality rate. Cardiac complications of sepsis are associated with a worse prognosis. Currently, there is no effective treatment for sepsis-induced cardiomyopathy. Studies using human tissue samples have shown that cardiomyocyte cell death is rare during sepsis and does not explain the decrease in systolic function (32). Despite years of research, the cellular mechanisms of systolic dysfunction during sepsis remain unclear (33). Multiple abnormalities have been reported, using cardiomyocytes and animal models, without the identification of a central mechanism. We used both in vivo and cellular model systems at early time points to identify the factors that initiate contractile dysfunction. We found that LPS is sufficient to rapidly increase mitochondrial superoxide and decrease contractility in isolated cardiomyocytes, and NOX2 activation is required for these abnormalities. Further, we show that in vivo inhibition of NOX2 protects mice from sepsis-induced systolic dysfunction using both the LPS-injection model and the CLP model of polymicrobial sepsis. We propose that sepsis activates cardiac NOX2, which increases sarcoplasmic reticulum calcium leak, impairing cardiomyocyte contractility and leading to mitochondrial dysfunction (Figure 8). NOX2 inhibition also reduces JNK activation and downregulation of metabolic genes (Figure 5).

Previous work has shown that exposing ventricular myocytes to higher doses of LPS for 24 hours is sufficient to reduce contractility (34). We used lower doses of LPS and early time points to identify the initiating factors that lead to sepsis-induced cardiomyopathy. We show that inhibition of NOX2 is protective in both isolated cardiomyocyte experiments and in animal models of sepsis. This is the first time to our knowledge that pharmacologic NOX2 inhibition has been shown to prevent sepsis-induced contractile dysfunction in vivo. A prior report showing that NOX2-KO hearts were protected from the harmful effects of LPS emphasized the role of inflammation (35). Our data demonstrate a potentially novel mechanism that links NOX2 activation with abnormal calcium handling and mitochondrial dysfunction. Importantly, NOX2 inhibition alleviated oxidative stress and preserved cardiac function without resolution of the inflammatory component of the disease based on serum cytokines, although apocynin may have an effect on WBC function. Thus, our study identifies a potentially novel role for NOX2 in the pathophysiology of the disease, acting through mitochondria and cardiac metabolism in a way that is largely independent of systemic inflammation.

NOX2 is known to transiently increase sarcoplasmic reticulum calcium release in cardiomyocytes in response to stretch (26). While this stretch response may be the physiologic function of cardiac NOX2, long-term activation of NOX2 may be maladaptive since it promotes arrhythmia (36) and heart failure (37). Previous work has demonstrated that sepsis increases sarcoplasmic reticulum calcium leak (sparks) in cardiomyocytes (23). Our experiments demonstrate that LPS is sufficient to increase calcium sparks. It is also possible that non–spark-mediated sarcoplasmic reticulum calcium leak contributes to the pathophysiology. We also demonstrate smaller calcium transients after LPS exposure, which can be a direct cause of decreased cardiac contractility, since calcium release is essential for sarcomere contraction. Smaller-amplitude calcium transients are characteristic of systolic heart failure of diverse etiologies (38).

We propose that sepsis causes mitochondrial dysfunction through increased sarcoplasmic reticulum calcium leak, which promotes mitochondrial calcium overload and partial depolarization of mitochondria. Mitochondrial dysfunction may contribute to decreased cardiac contractility. The beneficial effect of cyclosporin A in our experiments confirms that mPTP opening contributes to mitochondrial dysfunction during sepsis (39). Opening of the mPTP can be triggered by calcium overload (24). Increased calcium leak could also have harmful effects on cardiac transcription at later time points by activating NFAT and other calcium-sensitive transcriptional pathways, which have been associated with cardiac dysfunction (40).

Our data suggest that PKC-isoform activation is upstream of NOX activation in the heart. PKCβ is a consistent finding in the 2 models and this is probably the activator of NOX2. Although we show that NOX inhibition is effective at preserving contractility in vitro and in vivo, it is also possible that activation of PKC isoforms by LPS has harmful effects that are not mediated by NOX2. For example, the gene expression data from the CLP model indicate that PKC inhibition is more effective at normalizing metabolic gene expression than apocynin, the NOX inhibitor.

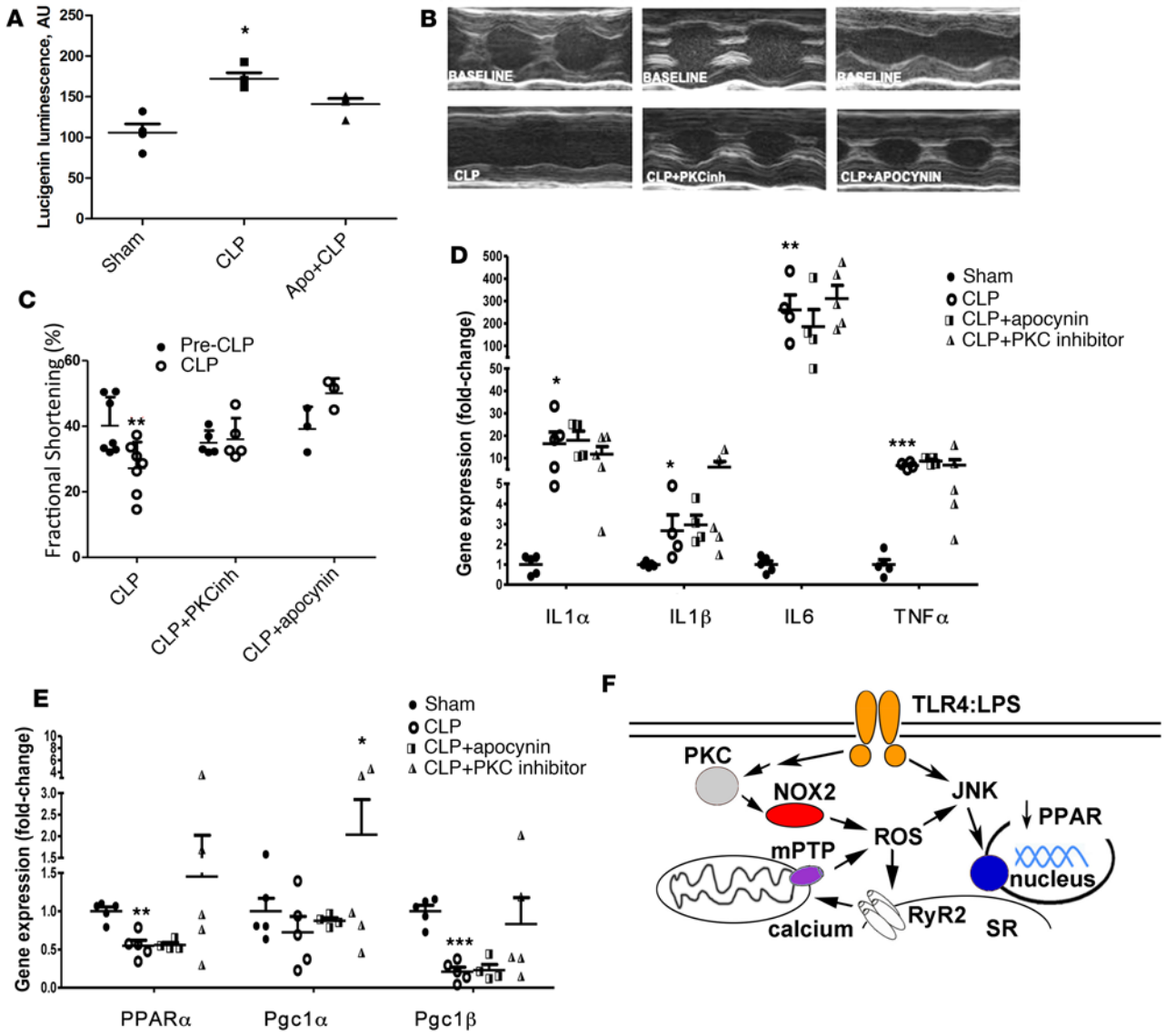

Figure 8. CLP model is also protected by inhibition of PKC or NOX; diagram of proposed pathway. (**A**) Graph of lucigenin (NOX activity) from ventricular tissue lysates. *n* = 4 mice per group. (**B**) Representative M-mode echocardiograms from C57BL/6 mice treated with vehicle control, PKC inhibitor Ro-31-8220, or apocynin, at the time of cecal ligation and puncture (CLP) surgery. (**C**) Graph of echo data before and after CLP surgery. (**D**) Graph of inflammatory gene expression from ventricular tissue, *n* = 4–5 mice per group. (**E**) Graph of metabolic gene expression from ventricular tissue, *n* = 4-5 mice per group. (**F**) Diagram of proposed pathway. $^{*}P < 0.05$, $^{**}P < 0.01$, $^{***}P < 0.001$ by ANOVA with post-hoc testing.

Although immune system activation may contribute to cardiac dysfunction in later stages of sepsis (41, 42), our experiments show that LPS has a rapid, direct toxic effect on cardiomyocytes. Furthermore, the NOX2 inhibitor apocynin prevents systolic dysfunction in vivo, but it does not cause a reduction in circulating proinflammatory cytokines or cardiac tissue inflammatory gene expression, demonstrating that cardiac contractility and systemic inflammation can be dissociated. This finding is consistent with our previous findings showing that induction of cardiac fatty acid oxidation and energy production improved cardiac function prior to alleviation of inflammation (11, 13). These new findings, in combination with our prior work, suggest a crucial role for restoration of mitochondrial function and cardiac energetics as a way to maintain cardiac function in sepsis, independently of systemic inflammation, at least for the early stage of the disease.

The fact that NOX activation during sepsis decreases expression of genes that are required for mitochondrial function is a potentially novel finding. We have previously shown that LPS-mediated JNK activation is responsible for the decrease in expression of *Pppara* and other genes required for fatty acid oxidation by mitochondria (13). NOX2 inhibition prevents activation of JNK, which improves the expression of these genes. We

also found that cardiac expression of Ucp2 and Ucp3 was upregulated in the mouse model of sepsis. UCPs are mitochondrial transporter proteins that create proton leaks across the inner mitochondrial membrane, thus uncoupling oxidative phosphorylation from ATP synthesis. Superoxide activates UCPs (43), and UCP activation may decrease mitochondrial superoxide production (44). Although this may be an adaptive response to increased oxidative stress, increased UCP activity and/or expression would tend to decrease cardiac efficiency by decreasing the mitochondrial inner membrane potential.

Although the NOX inhibitor apocynin did not improve mortality by itself in the rodent CLP model, it is possible that with intravenous fluid resuscitation and broad-spectrum antibiotics, NOX inhibitors could have additional benefit during septic shock complicated by cardiomyopathy. In conclusion, our results indicate that NOX2 activation is a critical factor in the pathophysiology of sepsis-induced cardiomyopathy, acting at least in part independently of systemic inflammation. NOX2 activation increases cardiac superoxide production, causes mitochondrial dysfunction, and decreases contractility. We used a small-molecule inhibitor of NOX2 in 2 different models of sepsis to demonstrate the potential for translational application of these findings. Although NOX2 inhibition could potentially reduce bactericidal functions of WBCs, it is possible that selective, partial inhibition of NOX2 in combination with antibiotics would be beneficial during sepsis.

Methods

Animal care, sepsis models, and cardiomyocyte isolation. WT and B6.129S-*Cybb*^{tm1Din}/J (NOX2-KO) mice were purchased from The Jackson Laboratory and were 8–12 weeks old at the time of experiments. LPS injections were performed as previously described (11) and animals were sacrificed 6–9 hours after LPS injections. Briefly, 5 mg/kg of LPS (Sigma-Aldrich), which is a sublethal dose, was administered by intraperitoneal injection. Control mice were treated with an equal volume of saline. Mice received a single intraperitoneal injection of 6 mg/kg Ro-31-8220 (Sigma-Aldrich) for PKC inhibition or 50 mg/kg apocynin for NOX inhibition. Both pharmacologic agents were administered 30 minutes prior to LPS injection. For CLP surgery, a 1- to 2-cm midline laparotomy was created to expose the cecum with the adjoining intestine. The cecum was ligated 1 cm from the distal end of the cecum. The cecum was punctured twice with a 19-gauge needle and gently squeezed so that a small amount of feces was extruded. Mice were resuscitated by injecting 1 ml of 0.9% saline solution subcutaneously. Mice were injected with inhibitor compounds at the time of surgery and again 6 hours later. Echocardiograms were performed 12 hours after CLP. Two-dimensional echocardiography was performed on anesthetized mice (inhaled isoflurane) using a VisualSonics Vevo 2100 machine. Echocardiographic images were recorded in a digital format. A single observer blinded to the respective treatments of mice then analyzed images off-line.

Cardiomyocyte isolation and measurements of ROS, mitochondrial calcium, and mitochondria depolarization. Cardiomyocytes were isolated from adult mouse hearts using established protocols (45). Briefly, the heart was removed and the aorta was cannulated. After calcium-free buffer was perfused for 2 minutes, collagenase (0.3 mg/ml; Liberase, Roche) solution was perfused through the coronary arteries for 7 minutes with calcium at 12.5 μM. Left ventricular tissue was teased apart and pipetted to release individual cells. After LPS and/or drug treatment, isolated cardiomyocytes were divided into aliquots. To measure ROS, cardiomyocytes were loaded with the fluorescent dye 2′,7′-dichlorofluorescin diacetate (DCF) (25 μM, Sigma-Aldrich) or MitoSOX Red (5 μM, Life Technologies), a mitochondrial superoxide indicator, was used to analyze mitochondrial superoxide generation within cardiomyocyte mitochondria, and incubated for 30 minutes in the dark. Excess DCF or MitoSOX Red was removed with 2 washes of BSA solution. DCF fluorescence was recorded at excitation/emission wavelengths of 488/532 nm, whereas MitoSOX Red was recorded at 525/620 nm. To assess the changes in mitochondrial membrane potential, cardiomyocytes were stained with 1 nM TMRM ester (Thermo Fisher Scientific) for 30 minutes and recorded at 543 nm (excitation)/590 nm (emission). TMRM preferentially accumulates inside mitochondria due to its positive charge. As mitochondria are depolarized, they trap less TMRM; thus, the signal is proportional to the inner membrane potential (46). To determine the changes in mitochondrial calcium in living cells, cardiomyocytes were loaded with 10 μM Rhod 2-AM (Thermo Fisher Scientific) and incubated for 30 minutes followed by 1-hour washout and cytosolic quenching with manganese, to produce a specific mitochondrial calcium signal (47). Rhod 2-AM fluorescence was measured at 552 nm (excitation)/581 nm (emission). Cells were loaded onto a 96-well plate in triplicate at 2,000 cells/well, and fluorescence was measured with a Tecan Infinite 200 plate reader.

Single-cell contractility and calcium transients. Only rod-shaped cardiomyocytes with clear striations that were not spontaneously contracting at baseline were selected for experiments. Myocytes were field stimulated at 1 Hz in a chamber contained Tyrode's solution with 1.8 mM $CaCl_2$ at room temperature. Imaging and quantification were performed using Ionoptix software Ionwizard 6.2. Sarcomere length measurements were performed using a fast Fourier transform algorithm. For experiments to evaluate calcium transients, cardiomyocytes were loaded with 1 μM fura-2 AM (Molecular Probes) for 10 minutes at room temperature, followed by two 10-minute washes. Calcium transients were quantified as the ratio of fura-2 emission.

Sparks and caffeine release experiments. Sparks were recorded with a Leica SP2 confocal microscope equipped with a 63× 1.4 NA objective. Cardiomyocytes were loaded with fluo-4-AM (5 μM, 10 minutes; Thermo Fisher Scientific), in modified Tyrode's solution containing 1 mM calcium. Line scan images were recorded with Leica TCS software and quantified with the Sparkmaster plugin of ImageJ (NIH). For caffeine release experiments, cardiomyocytes were loaded with Rhod 2-AM (5 μM with 0.05% Pluronic F127 detergent) in Tyrode's solution (containing in mM: 138 NaCl, 4 KCl, 2 $CaCl_2$, 1 $MgCl_2$, 0.33 NaH_2PO_4, and 10 HEPES) for 20 minutes at room temperature. Cells were then washed and maintained in Tyrode's. A Leica SP2 microscope equipped with a 63×, oil immersion, N.A. 1.4 objective was used for confocal line scan imaging. The electronic zoom was adjusted to fit the cells, and the scan field was rotated to be along the long axis of the cells. Static bright-field and fluorescence images were taken before measuring intracellular Ca^{2+} release. Rhod-2-AM was excited at 543 nm and emission detected between 550 and 600 nm. Confocal line scan frequency was set at 400 Hz. Cardiomyocytes were paced for 10 seconds, during which line scan images of normal Ca^{2+} transients were acquired. Following this, pacing was stopped and 10 mM caffeine solution was perfused into the dish. As soon as sarcoplasmic reticulum Ca^{2+} release was observed, perfusion was switched to normal Tyrode's solution.

Cell culture. H9c2 cells were purchased from ATCC and cultured in DMEM with 10% FBS. Oxygen consumption rate (OCR) was measured with an XF24 Extracellular Flux Analyzer (Agilent Technologies, Seahorse Bioscience). H9c2 cells were seeded in an XF 24-well cell culture microplate at a density of 2,000 cells/well. For Seahorse experiments, the following inhibitors were used: 1 μm oligomycin, 750 nM FCCP, 1 μm rotenone, and 1 μm antimycin-A in the same injection port.

Histology. Freshly isolated ventricular tissue sections were loaded with dihydroethidium (150 μm) in serum-free media for 30 minutes at room temperature with shaking at 30 rpm, to visualized ROS. NADPH autofluorescence was acquired using a 2-photon laser at 720 nm excitation and emission at 380–550 nm. Images were acquired using a Zeiss 710 Microscope equipped with 10× objective and a Coherent Chameleon 2-photon laser (48).

NOX activity. NADPH-dependent superoxide production was measured in cellular homogenates using lucigenin-enhanced chemiluminescence as previously described (49). Cells were homogenized in Kreb's buffer, pH 7.4 (130 mM NaCl, 5 mM KCl, 2 mM $MgCl_2$, 1.5 mM $CaCl_2$, 5 mM glucose, 35 mM phosphoric acid, and 20 mM HEPES). Homogenates were centrifuged at 1,000 *g* at 4°C for 10 minutes to remove the unbroken cells and debris. The pellet was resuspended in Kreb's buffer containing 0.5 mM lucigenin followed by the addition of 0.1 mM NADH as the substrate. Protein content was measured using the Bradford protein assay reagent. The samples were transferred to a 96-well plate at 50 μg of protein per well. Photon emission in terms of relative light units was measured in a Tecan 200 microplate reader after a 5-minute incubation in the dark. There was no measurable activity in the absence of NADPH. Superoxide anion production was expressed as relative lucigenin luminescence. gp91ds-tat was purchased from Anaspec. Go6983 was purchased from Tocris.

RNA purification and gene expression analysis. Total RNA was purified from cells or hearts using TRIzol reagent according to the manufacturer's instructions (Invitrogen). DNase-treated RNA was used for cDNA synthesis using the ProtoScript II First-Strand cDNA Synthesis Kit (New England Biolabs). Quantitative real-time PCR was performed with the SYBR Select Master Mix (Applied Biosystems). Incorporation of the SYBR green dye into the PCR products was monitored in real time with an Mx3000 sequence detection system (Stratagene). Samples were normalized against 18S ribosomal RNA. The sequences of the primers have been described previously (11).

Protein purification and analysis. Isolated heart tissues or cells were homogenized in radioimmune precipitation assay buffer containing protease inhibitors (1 mM benzamidine, 1 mM phenylmethylsulfonyl fluoride, 10 μg/ml leupeptin, 10 μg/ml aprotinin, 5 mM ethylene glycol tetraacetic acid, and 2 mM ethylene diamine tetraacetic acid; Sigma-Aldrich) as well as 1 mM dithiothreitol and phosphatase inhibitors

(Halt phosphatase inhibitor mixture, Thermo Fisher Scientific). Total protein extract was applied (25 μg) to SDS-PAGE and transferred onto nitrocellulose membranes. Antibodies were obtained from Millipore (PKCα, 05-154), Santa Cruz Biotechnology (β-actin, C4sc47778; JNK, D2sc7345; PKCβ, E3sc8049; PKCδ, C17sc213; and PKCε, E5sc1681), and Cell Signaling Technology (phospho-PKCδ, 9374S; phospho-JNK, 2993S; phospho-JNK-Ser-63, 9261S; phospho-JNK-Ser-73, 9164S; and phospho-ERK, 9101).

Multiplex cytokine and phosphoprotein analysis. Cytokine concentrations in mouse serum were determined using the mouse cytokine/chemokine magnetic bead panel (Millipore) according to the manufacturer's instructions. The final data were obtained and analyzed via the Bioplex Magpix multiplex reader system (Bio-Rad). Loading for the protein panels was normalized via determination of total protein concentration (BCA Protein Assay kit, Pierce).

Measurement of WBC count. We used ACK buffer-erythrocyte lysis buffer to isolate WBCs from total blood, incubated for 5–10 minutes on a rocker. This was followed by adding an equal volume of cold phosphate-buffered saline (PBS), centrifuging at 300 *g* for 5 minutes at 2°C–8°C, and discarding the supernatant. The pellet was resuspended with ACK lysis buffer. We measured the WBCs using the TC20 Automated Cell Counter from Bio-Rad.

Statistics. Results are presented as the mean ± SEM. The unpaired *t* test was used for comparisons of 2 means; a 2-tailed *P* value of less than 0.05 was considered statistically significant. For groups of 2 or more ANOVA was used with post-hoc testing (Prism v5, GraphPad Software).

Study approval. Animal protocols were reviewed and approved by the Columbia University and Temple University Institutional Animal Care and Use Committees (New York, NY and Philadelphia, PA, respectively) and were carried out in accordance with the NIH guidelines for the care and use of laboratory animals.

Author contributions

LCJ, DK, MCV, EB, DT, NEH, MH, AJR, MM, KD, and JPM designed the research. LCJ, DK, MCV, EB, DT, GJK, SP, NEH, KD, and JPM performed the research. LCJ, EB, NEH, PS, HMC, MH, AJR, MM, KD, and JPM analyzed the data. AJR, MM, KD, and JPM wrote the manuscript.

Acknowledgments

This work was supported by T32 HL007343 to LCJ, K08 HL105801 to JPM; R00 HL112853 and R01 HL130218 to KD; R01 GM109882, R01 HL086699, R01 HL119306, and 1S10 RR027327 to MM; and AJR is supported by NIH R01 AI092743, R21 AI111020, and R33 AI098654. DT is supported by AHA postdoctoral fellowship (17POST33660251).

Address correspondence to: John P. Morrow, Division of Cardiology, Columbia University College of Physicians and Surgeons, PH 10-203, 622 W 168th St, New York, New York 10032, USA. Phone: 212.305.5553. Email: jpm46@cumc.columbia.edu. Or to: Konstantinos Drosatos, Metabolic Biology Laboratory, Lewis Katz School of Medicine at Temple University, Deparment of Pharmacology Center for Translational Medicine, 3500 N. Broad St, MERB-951, Philadelphia, Pennsylvania 19140, USA. Phone: 215.707.1421; Email: drosatos@temple.edu.

1. Angus DC, van der Poll T. Severe sepsis and septic shock. *N Engl J Med*. 2013;369(21):2063.
2. Kalla C, Raveh D, Algur N, Rudensky B, Yinnon AM, Balkin J. Incidence and significance of a positive troponin test in bacteremic patients without acute coronary syndrome. *Am J Med*. 2008;121(10):909–915.
3. Boyd JH, Mathur S, Wang Y, Bateman RM, Walley KR. Toll-like receptor stimulation in cardiomyoctes decreases contractility and initiates an NF-kappaB dependent inflammatory response. *Cardiovasc Res*. 2006;72(3):384–393.
4. Andersson DC, et al. Mitochondrial production of reactive oxygen species contributes to the β-adrenergic stimulation of mouse cardiomycytes. *J Physiol (Lond)*. 2011;589(Pt 7):1791–1801.
5. Mehta S, et al. Agreement in electrocardiogram interpretation in patients with septic shock. *Crit Care Med*. 2011;39(9):2080–2086.
6. Rich MM, McGarvey ML, Teener JW, Frame LH. ECG changes during septic shock. *Cardiology*. 2002;97(4):187–196.
7. Makrygiannis SS, et al. Incidence and predictors of new-onset atrial fibrillation in noncardiac intensive care unit patients. *J Crit Care*. 2014;29(4):697.e1–697.e5.
8. Kamisoglu K, et al. Human metabolic response to systemic inflammation: assessment of the concordance between experimental endotoxemia and clinical cases of sepsis/SIRS. *Crit Care*. 2015;19:71.
9. Xu C, Yi C, Wang H, Bruce IC, Xia Q. Mitochondrial nitric oxide synthase participates in septic shock myocardial depression by nitric oxide overproduction and mitochondrial permeability transition pore opening. *Shock*. 2012;37(1):110–115.
10. Ichinose F, et al. Cardiomyocyte-specific overexpression of nitric oxide synthase 3 prevents myocardial dysfunction in murine

models of septic shock. *Circ Res*. 2007;100(1):130–139.
11. Drosatos K, et al. Peroxisome proliferator-activated receptor-γ activation prevents sepsis-related cardiac dysfunction and mortality in mice. *Circ Heart Fail*. 2013;6(3):550–562.
12. Schilling J, Lai L, Sambandam N, Dey CE, Leone TC, Kelly DP. Toll-like receptor-mediated inflammatory signaling reprograms cardiac energy metabolism by repressing peroxisome proliferator-activated receptor γ coactivator-1 signaling. *Circ Heart Fail*. 2011;4(4):474–482.
13. Drosatos K, et al. Inhibition of c-Jun-N-terminal kinase increases cardiac peroxisome proliferator-activated receptor alpha expression and fatty acid oxidation and prevents lipopolysaccharide-induced heart dysfunction. *J Biol Chem*. 2011;286(42):36331–36339.
14. Zorov DB, Filburn CR, Klotz LO, Zweier JL, Sollott SJ. Reactive oxygen species (ROS)-induced ROS release: a new phenomenon accompanying induction of the mitochondrial permeability transition in cardiac myocytes. *J Exp Med*. 2000;192(7):1001–1014.
15. Hotchkiss RS, Karl IE. Dantrolene ameliorates the metabolic hallmarks of sepsis in rats and improves survival in a mouse model of endotoxemia. *Proc Natl Acad Sci USA*. 1994;91(8):3039–3043.
16. Zhang Y, Hu N, Hua Y, Richmond KL, Dong F, Ren J. Cardiac overexpression of metallothionein rescues cold exposure-induced myocardial contractile dysfunction through attenuation of cardiac fibrosis despite cardiomyocyte mechanical anomalies. *Free Radic Biol Med*. 2012;53(2):194–207.
17. Biary N, Xie C, Kauffman J, Akar FG. Biophysical properties and functional consequences of reactive oxygen species (ROS)-induced ROS release in intact myocardium. *J Physiol (Lond)*. 2011;589(Pt 21):5167–5179.
18. Heard SO, Toth IE, Perkins MW, Leonard JL. The role of protein kinase C in lipopolysaccharide-induced myocardial depression in guinea pigs. *Shock*. 1994;1(6):419–424.
19. Yang SL, Hsu C, Lue SI, Hsu HK, Yang J, Liu MS. Protein kinase C activity is increased in rat heart during the early hyperdynamic phase of sepsis. *Shock*. 1998;9(3):199–203.
20. Murphy MP. How mitochondria produce reactive oxygen species. *Biochem J*. 2009;417(1):1–13.
21. Brand MD, Nicholls DG. Assessing mitochondrial dysfunction in cells. *Biochem J*. 2011;435(2):297–312.
22. Williams GS, Boyman L, Chikando AC, Khairallah RJ, Lederer WJ. Mitochondrial calcium uptake. *Proc Natl Acad Sci USA*. 2013;110(26):10479–10486.
23. Zhu X, et al. Increased leakage of sarcoplasmic reticulum Ca^{2+} contributes to abnormal myocyte Ca^{2+} handling and shortening in sepsis. *Crit Care Med*. 2005;33(3):598–604.
24. Halestrap AP. A pore way to die: the role of mitochondria in reperfusion injury and cardioprotection. *Biochem Soc Trans*. 2010;38(4):841–860.
25. Zhu H, Shan L, Peng T. Rac1 mediates sex difference in cardiac tumor necrosis factor-alpha expression via NADPH oxidase-ERK1/2/p38 MAPK pathway in endotoxemia. *J Mol Cell Cardiol*. 2009;47(2):264–274.
26. Prosser BL, Ward CW, Lederer WJ. X-ROS signaling: rapid mechano-chemo transduction in heart. *Science*. 2011;333(6048):1440–1445.
27. Joseph LC, et al. Inhibition of NAPDH oxidase 2 (NOX2) prevents oxidative stress and mitochondrial abnormalities caused by saturated fat in cardiomyocytes. *PLoS ONE*. 2016;11(1):e0145750.
28. Doi K, Leelahavanichkul A, Yuen PS, Star RA. Animal models of sepsis and sepsis-induced kidney injury. *J Clin Invest*. 2009;119(10):2868–2878.
29. Drosatos K, Lymperopoulos A, Kennel PJ, Pollak N, Schulze PC, Goldberg IJ. Pathophysiology of sepsis-related cardiac dysfunction: driven by inflammation, energy mismanagement, or both? *Curr Heart Fail Rep*. 2015;12(2):130–140.
30. Jaishy B, et al. Lipid-induced NOX2 activation inhibits autophagic flux by impairing lysosomal enzyme activity. *J Lipid Res*. 2015;56(3):546–561.
31. Moon JS, et al. UCP2-induced fatty acid synthase promotes NLRP3 inflammasome activation during sepsis. *J Clin Invest*. 2015;125(2):665–680.
32. Takasu O, et al. Mechanisms of cardiac and renal dysfunction in patients dying of sepsis. *Am J Respir Crit Care Med*. 2013;187(5):509–517.
33. Merx MW, Weber C. Sepsis and the heart. *Circulation*. 2007;116(7):793–802.
34. Hobai IA, Morse JC, Siwik DA, Colucci WS. Lipopolysaccharide and cytokines inhibit rat cardiomyocyte contractility in vitro. *J Surg Res*. 2015;193(2):888–901.
35. Peng T, Lu X, Feng Q. Pivotal role of gp91phox-containing NADH oxidase in lipopolysaccharide-induced tumor necrosis factor-alpha expression and myocardial depression. *Circulation*. 2005;111(13):1637–1644.
36. Kim YM, et al. A myocardial Nox2 containing NAD(P)H oxidase contributes to oxidative stress in human atrial fibrillation. *Circ Res*. 2005;97(7):629–636.
37. Zhang M, Perino A, Ghigo A, Hirsch E, Shah AM. NADPH oxidases in heart failure: poachers or gamekeepers? *Antioxid Redox Signal*. 2013;18(9):1024–1041.
38. Kranias EG, Hajjar RJ. Modulation of cardiac contractility by the phospholamban/SERCA2a regulatome. *Circ Res*. 2012;110(12):1646–1660.
39. Larche J, et al. Inhibition of mitochondrial permeability transition prevents sepsis-induced myocardial dysfunction and mortality. *J Am Coll Cardiol*. 2006;48(2):377–385.
40. Gandhirajan RK, et al. Blockade of NOX2 and STIM1 signaling limits lipopolysaccharide-induced vascular inflammation. *J Clin Invest*. 2013;123(2):887–902.
41. Riedemann NC, Guo RF, Ward PA. The enigma of sepsis. *J Clin Invest*. 2003;112(4):460–467.
42. Kumar A, Thota V, Dee L, Olson J, Uretz E, Parrillo JE. Tumor necrosis factor alpha and interleukin 1beta are responsible for in vitro myocardial cell depression induced by human septic shock serum. *J Exp Med*. 1996;183(3):949–958.
43. Echtay KS, et al. Superoxide activates mitochondrial uncoupling proteins. *Nature*. 2002;415(6867):96–99.
44. Modrianský M, Gabrielová E. Uncouple my heart: the benefits of inefficiency. *J Bioenerg Biomembr*. 2009;41(2):133–136.
45. Morrow JP, et al. Mice with cardiac overexpression of peroxisome proliferator-activated receptor γ have impaired repolarization and spontaneous fatal ventricular arrhythmias. *Circulation*. 2011;124(25):2812–2821.

46. Ichas F, Jouaville LS, Mazat JP. Mitochondria are excitable organelles capable of generating and conveying electrical and calcium signals. *Cell*. 1997;89(7):1145–1153.
47. Pan X, et al. The physiological role of mitochondrial calcium revealed by mice lacking the mitochondrial calcium uniporter. *Nat Cell Biol*. 2013;15(12):1464–1472.
48. Vagnozzi RJ, et al. Inhibition of the cardiomyocyte-specific kinase TNNI3K limits oxidative stress, injury, and adverse remodeling in the ischemic heart. *Sci Transl Med*. 2013;5(207):207ra141.
49. Bendall JK, Cave AC, Heymes C, Gall N, Shah AM. Pivotal role of a gp91(phox)-containing NADPH oxidase in angiotensin II-induced cardiac hypertrophy in mice. *Circulation*. 2002;105(3):293–296.